

Observed changes of global and western Pacific precipitation associated with global warming SST mode and mega-ENSO SST mode

Byeong-Hee Kim · Kyung-Ja Ha

Received: 30 June 2014 / Accepted: 13 February 2015 / Published online: 22 February 2015
© Springer-Verlag Berlin Heidelberg 2015

Abstract Changes in the observed precipitation and moisture transport induced by anthropogenic forcing and natural variability were investigated. To separate into the anthropogenic and natural modes, the multi-variate EOF (MVEOF) analysis synthesized from three variables including of precipitation, SST, and moisture flux convergence is used. The precipitation pattern over the tropics has a tri-polar structure in anthropogenic mode but a zonal asymmetric structure near 150°E in natural mode. The patterns of precipitation were determined in the principal modes of moisture flux convergence using MVEOF. Through a moisture budget analysis, the dynamic factor of moisture flux was found to play an important role in the precipitation changes. The natural and anthropogenic modes have zonal wave patterns of potential function associated with the dynamic factor: zonal wavenumber 1 and 2 structure, respectively. When the decadal ENSO is in mega-La Niña phase, natural and anthropogenic forcings represent a positive sign of potential function, which means increased precipitation over the tropical western Pacific (WP). In the tropics, anthropogenic forcing slightly strengthens westerly winds over the Indian Ocean and easterly winds over the WP, while weaken the easterly winds over the eastern Pacific. The natural variability strengthens the Walker circulation in La Niña phase. Therefore, during recent three decades, the slightly strengthening of the wind convergence near the WP by anthropogenic forcing and the strengthening of the Walker circulation by natural variability have caused the increasing precipitation over the WP.

Keywords Anthropogenic forcing · Moisture flux · MVEOF · Natural variability · Precipitation · Walker circulation

1 Introduction

Developing an understanding of changes in precipitation is important because such changes are closely related to human activity. Studies of precipitation change have been focused mainly at regional scales, such as that of monsoons, because of their indigenous characteristics. Such dominant monsoon systems on Earth include the Asian, Australian, African, and American monsoons. (Tao and Chen 1987; McBride 1987; Nicholson and Kim 1997; Webster et al. 1998; Zhou and Lau 1998; Higgins et al. 2003). Although many studies have addressed the question of recent changes in monsoons, the results have relied on different measures of monsoon strength. However, in its physical essence, monsoons are a forced response of the climate system. Land–sea thermal contrast is critical for determining the location and strength of a monsoon, but it is neither a necessary nor sufficient condition. Therefore, an understanding of global precipitation change is required.

Observed land precipitation decreased from 1950 to 1980 but leveled off after 1980 (Higgins et al. 2003; Wang and Ding 2006; Polson et al. 2013). In recent three decades (i.e., since 1979), satellite estimates of oceanic rainfall have revealed an increasing trend (Shon et al. 2004; Hsu et al. 2011; Wang et al. 2012). Several studies have noted that global monsoon precipitation has been increasing during the period 1979–2008 (Wang et al. 2012; Hsu et al. 2011; Lee et al. 2014). Precipitation variability studies conducted previously have mostly determined the ways in which global precipitation has responded to the last 30 years of

B.-H. Kim · K.-J. Ha (✉)
Division of Earth Environmental System,
Pusan National University, Busan, Korea
e-mail: kjha@pusan.ac.kr

rapid global warming. However, owing to the lack of observations over the oceans before 1979, long-term change of global precipitation could not be fully understood until recently.

To understand changes in precipitation at the global scale, including oceanic areas, such changes have been studied primarily by using global climate models. Through global climate model projection under global warming, a robust signal of increased global precipitation has been detected (Held and Soden 2006; Chou et al. 2009; Seager et al. 2010; Cherchi et al. 2011; Hsu et al. 2012; Lee and Wang 2014; Lee et al. 2014). Whether this increasing trend will continue into a future potentially warmer climate throughout the twenty first century is an important issue that needs to be addressed.

However, recent studies have suggested that natural variability plays an important role, as large as that of global warming, in long-term precipitation change (Hoerling et al. 2010; Wang et al. 2012, 2013; Liu et al. 2013; Marvel and Bonfils 2013). To predict future changes in precipitation, the relative roles of natural variability and global warming on the recent global precipitation increase must be resolved, particularly over the western Pacific. Recently, this has become an important but unanswered issue.

To solve this problem, this study intended to investigate the relative roles of global warming and natural variability in observed change in the global precipitation and dynamically interpret global long-term variability. The rest of this paper is organized in the following manner. Section 2 introduces the data and methods used in the study. Section 3 investigates the change in precipitation related to global warming and natural variability. Section 4 presents an analysis of global warming and natural variability by using a diagnosis of the moisture budget, and Sect. 5 contains a summary and discussion.

2 Data and methods

2.1 Data

The reanalysis physical variables used in this study include daily specific humidity (q) and the northward and eastward wind components (u , v), respectively, at 8 atmospheric levels (1000, 925, 850, 700, 600, 500, 400, and 300 hPa). The data were obtained from the NCEP/NCAR reanalysis (NCEP1: Kalnay et al. 1996) and the European Centre for Medium-Range Weather Forecasts (ECMWF) reanalysis (ERA), which is a combination of the 40-year reanalysis (ERA-40, Uppala et al. 2005) and Interim reanalysis (ERA-Interim, Dee et al. 2011). Sea level pressure (SLP) was used for vertical integration from the datasets.

For monthly sea surface temperature (SST) data analysis, the Hadley Centre Sea Ice and SST (HadISST, Parker et al. 1999) and the extended reconstructed SST version 3 (ERSST-V3, Smith et al. 2008) were used. A monthly precipitation dataset was also obtained from NOAA's precipitation reconstruction dataset (NOAAP, Chen et al. 2002). The NOAAP data cover both land and ocean.

These datasets cover different time periods and were produced by different numerical models or assimilation systems. Thus, in order to obtain a robust result, we used the ensemble average of results obtained from different data. All the datasets were interpolated to a common 2.5° lat \times 2.5° lon grid by using a bilinear interpolation technique and merged for each variable during the period 1958–2012.

2.2 Moisture budget equation

The moisture budget is composed mainly of the local changes of total precipitable water (TPW), moisture transport (Q), precipitation (P), and evaporation (E). P minus E should maintain an approximate balance with the quantity Δ TPW and convergence of vertical integrated moisture flux (CVIMF, $-\nabla \cdot Q$) (Trenberth and Guillemot 1995). This can be written as

$$P - E = -\frac{\partial(\text{TPW})}{\partial t} - \nabla \cdot Q. \quad (1)$$

We should measure the vertical integrated local moisture and moisture transport,

$$\text{TPW} = \frac{1}{g} \int_{p_s}^{p_t} q \, dp \quad (2)$$

and

$$Q = \frac{1}{g} \int_{p_s}^{p_t} (q\mathbf{V}) \, dp, \quad (3)$$

where q is specific humidity, \mathbf{V} is the horizontal wind vector, p is pressure, p_s is surface pressure, p_t is top pressure, and g is the acceleration of gravity.

Assuming that the rates of change of TPW and condensates are small over a sufficiently long period, CVIMF is balanced by precipitation minus evaporation. Thus Eq. (1) can be written as

$$-\nabla \cdot \bar{Q} = \bar{P} - \bar{E}. \quad (4)$$

In this study, $\bar{(\)}$ denotes the annual average. Thus, CVIMF has a key role in the hydrological cycle pertaining to moisture source and sink.

CVIMF can be divided into three terms: a moisture convergence term, a moisture advection term, and an eddy term, as shown below.

$$-\nabla \cdot \bar{Q} = - \left[\frac{1}{g} \int_{p_t}^{p_s} (\bar{q} \nabla \cdot \bar{V}) dp \right] - \left[\frac{1}{g} \int_{p_t}^{p_s} (\bar{V} \cdot \nabla \bar{q}) dp \right] - \left[\frac{1}{g} \int_{p_t}^{p_s} (\nabla \cdot \bar{q}' \bar{V}') dp \right] \tag{5}$$

The first term on the right side is the moisture convergence term. If the wind is undergoing convergence (divergence), it has a positive (negative) contribution to CVIMF. The second term on the right is the moisture advection term. When it is positive (negative), i.e., the wind flows from a wet (dry) region to dry (wet) region, CVIMF has a positive (negative) contribution. The last term on the right side is the eddy term. The convergence term and the advection term are usually referred as the dynamic and thermodynamic components in moisture transport, respectively.

2.3 Divergent and non-divergent components

In this study, by separating the moisture transport vector into divergent (Q_D) and non-divergent (Q_R) components (Rosen et al. 1979; Chen 1985; Sohn et al. 2004) and introducing the moisture flux potential function (χ_Q), moisture transport was solved for, that is,

$$-\nabla \cdot \bar{Q} = \bar{P} - \bar{E} = -\nabla^2 \bar{\chi}_Q \tag{6}$$

$$\bar{Q}_D = \nabla \bar{\chi}_Q \tag{7}$$

Equations (6) and (7) were solved on a complete global domain using the spectral method. The non-divergent component describes mostly the large-scale moisture transport, and the use of Eqs. (6) and (7) is more appropriate for investigating the hydrological cycle directly linking source to sink regions.

3 Principal coupling modes of global precipitation, SST, and CVIMF

Assuming that SST can influence long-term global precipitation change, as suggested in previous studies (Ropelewski and Halpert 1996; Cobb et al. 2003; Yun et al. 2010; Liu et al. 2013), the leading “coupled” mode of the 3-year running mean of annual averaged precipitation and the underlying SST field derived by singular value decomposition (hereafter, SVD1) during the period 1958–2012 explains about 71.57 % of the total covariance between the two fields (Fig. 1). Global precipitation shows a zonal asymmetric pattern near 150°E, and the SST pattern and its relationship to the pattern of precipitation resemble a La Niña-like distribution (Fig. 1a, b). The time series show decadal or multi-decadal variation and a positive linear trend (Fig. 1c).

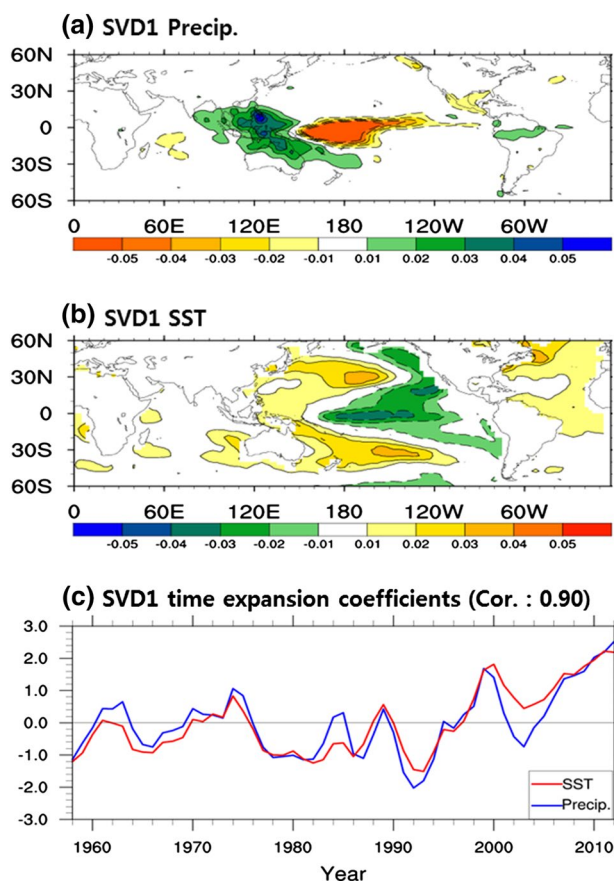
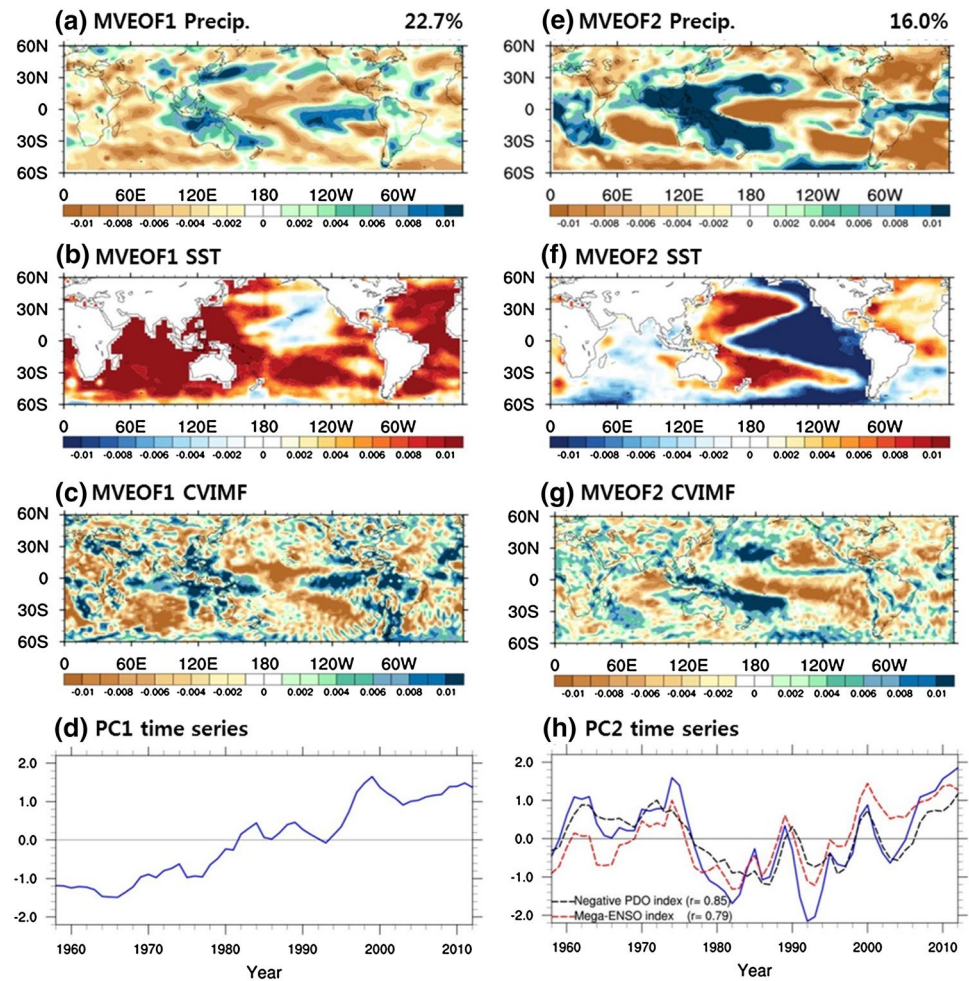


Fig. 1 The leading SVD modes and time expansion coefficients for the 3-year running means of annual averaged precipitation and SST during the period 1958–2012 over the globe [60°S–60°N, 0–360°E]. SVD1 explains 71.57 % of the total covariance between precipitation and SST

The global precipitation pattern and evolution in SVD1 are similar to those in the first empirical orthogonal function (EOF) of precipitation, with spatial and temporal correlation coefficients of 0.89 and 0.99, respectively (not shown). In contrast, the SST has two dominant modes identified by EOF analysis. One is associated with global warming related to a long-term positive trend, the other is a pattern resembling the decadal El Niño–Southern Oscillation (ENSO) (Wang et al. 2012, 2013; Dong and Zhou 2014a; Dong et al. 2014). However, the SVDs for precipitation and SST have difficulty defining separated modes by global warming and decadal ENSO because the covariance of precipitation and SST in SVD is driven by larger variability of precipitation than that of SST. Basically changes in precipitation in a long time scale can be controlled by temperature, which related with Clausius-Clapeyron equation. However, the important term in a regional scale is circulation-based moisture transport, which can be divided by the circulation as a dynamic component and advection of moisture as a

Fig. 2 The first (*left panel*) and second (*right panel*) MVEOF modes and principal components (*blue solid line*) of the 3-year running means of annual averaged precipitation, SST, and CVIMF during the period 1958–2012 over the globe [60°S–60°N, 0–360°E]. For comparison, the 3-year running averaged negative PDO index (*black dashed line*) and mega-ENSO index (*red dashed line*) are shown in panel (**h**)

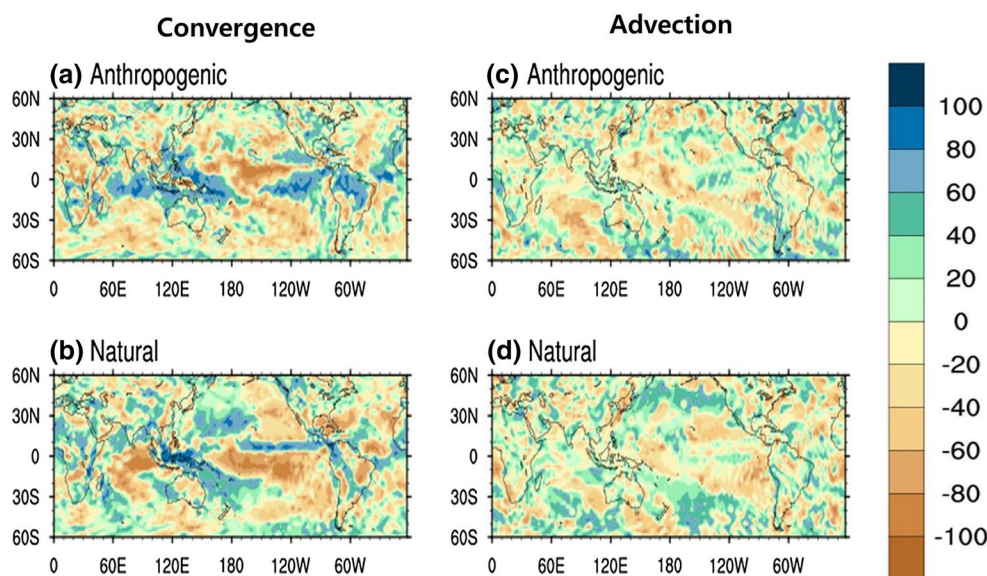


thermodynamic component. Thus, the precipitation reacts to the change of the dynamic and thermodynamic components. As mentioned in Sect. 2.2, the CVIMF include the dynamic and thermodynamic factors. To obtain the coherent patterns related to precipitation, SST and CVIMF, the multi-variate EOF (MVEOF) synthesized from the three variables was used. Figure 2 shows the first and second MVEOF (hereafter, MVEOF1 and MVEOF2) modes and the principal components (PCs) of the 3-year running mean of annual averaged precipitation, SST, and CVIMF during the period 1958–2012 over the globe [60°S–60°N, 0–360°E]. The MVEOF1 and MVEOF2 modes account for 22.7 and 16.0 % of the total variance, respectively. The first and second PCs (hereafter, PC1 and PC2) of MVEOF show a long-term positive trend and decadal variability, respectively (Fig. 2d, h). To compare PC2 with decadal oscillation indices of SST, the negative Pacific decadal oscillation (PDO) and mega-ENSO index were used. The PDO index was obtained from the Joint Institute for the Study of the Atmosphere and Ocean (JISAO, <http://jisao.washington.edu/pdo>). The mega-ENSO index is defined as the SST difference between the western Pacific K-shaped area

and the eastern Pacific triangle (Wang et al. 2013). The mega-ENSO is similar to ENSO, but it has a larger spatial scale and longer time scale. PC2 is highly correlated with the negative PDO ($r = 0.85$) and the mega-ENSO index ($r = 0.79$) (Fig. 2h). Thus, the MVEOF2 mode can be seen the natural mode, whereas the MVEOF1 mode have a long-term positive trend by anthropogenic forcing. Therefore, the two modes of MVEOF are referred to the anthropogenic mode and natural mode, respectively. The SST pattern of the MVEOF1 mode shows a general warming over global oceans except for the North Pacific, whereas the SST pattern of the MVEOF2 mode is quite similar to the mega-ENSO distribution (Fig. 2b, f).

The precipitation pattern of MVEOF1 shows a tri-polar distribution in the tropics, whereas SST is warming globally (Fig. 2a). Positive anomalies of precipitation appear over the western Pacific (WP) and eastern Pacific (EP), while negative anomalies appear over the central Pacific (CP). The pattern of precipitation of MVEOF2 is a distinct zonal asymmetric structure near 150°E (Fig. 2e). This pattern can be seen as an influence of the zonal asymmetric distribution of SST, in particular over the tropics (Fig. 2f).

Fig. 3 Ratio (%) fields of convergence (*left panel*) and advection (*right panel*) terms to CVIMF against the anthropogenic (*top panel*) and natural (*middle panel*) modes



The warm and cold SST lead to the anomalous low and high pressure over the tropics, respectively. The zonal pressure gradient drives the easterly wind anomaly over the tropics (Fig. 6c), and eventually the moisture is transported from EP to WP, and the WP can have an increasing rainfall. Through the Fig. 2a, e, anthropogenic forcing and natural variability are caused of the increased precipitation over the WP in recent 30 years (Wang et al. 2012, 2013). Especially, the influence of natural variability is broad and strong than that of global warming over the tropical WP in precipitation change. According to previous study, the influence of Interdecadal Pacific Oscillation (IPO) phase transition dominated than that of global warming over the Asian monsoon region during 1979–2008 (Dong and Zhou 2014b). The natural variability has a large influence on the changes in precipitation. Thus, the relative role of natural variability must be considered to improve the predictability of future climate change in precipitation. The characteristics of the precipitation patterns are also shown in the CVIMF patterns, especially over the tropics (Fig. 2c, g). Because the precipitation reacts to the change of the CVIMF in moisture budget equation, the CVIMF changes are important to precipitation changes, especially over the tropics.

To investigate the contributions of the dynamic and thermodynamic effects in CIVMF change, the ratio fields of the moisture convergence and advection terms to CVIMF are shown in Fig. 3. The eddy effect is not shown because it is smaller than those of the others. For global precipitation change, the moisture convergence (dynamic) component is more dominant than the moisture advection (thermodynamic) component in both the anthropogenic and natural modes. This result is consistent with the results of previous theoretical and modeling studies (Held and Soden

2006; Chou et al. 2009; Seager et al. 2010; Cherchi et al. 2011; Lin et al. 2014). Thus, the long-term trend and decadal variability of global precipitation are dominated by the dynamic component. Also, in middle latitude, the thermodynamic component ratio in anthropogenic mode is smaller than in natural mode (Fig. 3c, d). However, at the regional scale, the thermodynamic and eddy effects cannot be ignored in change of precipitation.

4 Attribution to changes in moisture budget components

The detailed dynamic component changes in the moisture budget are investigated in this section because the component mainly drives the change of CVIMF in both the anthropogenic and natural modes. Moisture source and sink regions are related to divergent winds of the dynamic component; thus, precipitation changes are investigated by the divergent component of moisture flux. Figure 4 shows that the potential function and divergent component of moisture flux are regressed by PC1 and PC2. The potential function pattern of the MVEOF1 mode has a zonal wave number 2 structure, whereas the MVEOF2 mode has an east–west pattern around the date line. The WP regions obtain moisture by both anthropogenic forcing and natural variability in the La Niña phase. However, if the distribution of SST is an El Niño pattern, it can disturb the increasing of precipitation over the WP, and the increased precipitation occurs over the EP. Such distributions of zonal wave patterns establish a great zonal transport band. Particularly, over the tropics, eastward (westward) moisture transport by divergent wind is dominant from the CP (EP) to the EP (WP) in anthropogenic (natural) mode.

Fig. 4 Regressed pattern of total (*top panel*), stationary (*middle panel*), and eddy (*bottom panel*) for the potential function (contour, 10^7 kg s^{-1}) and divergent component (vector, $\text{kg m}^{-1} \text{ s}^{-1}$) of vertical integral moisture flux with regard to **a** the anthropogenic (PC1, *left panel*) mode and **b** the natural (PC2, *right panel*) mode, respectively. Significance levels of 95 % about the potential function are shown in shading. Vector fields are shown since significance exceeds 95 % by the Student's *t* test

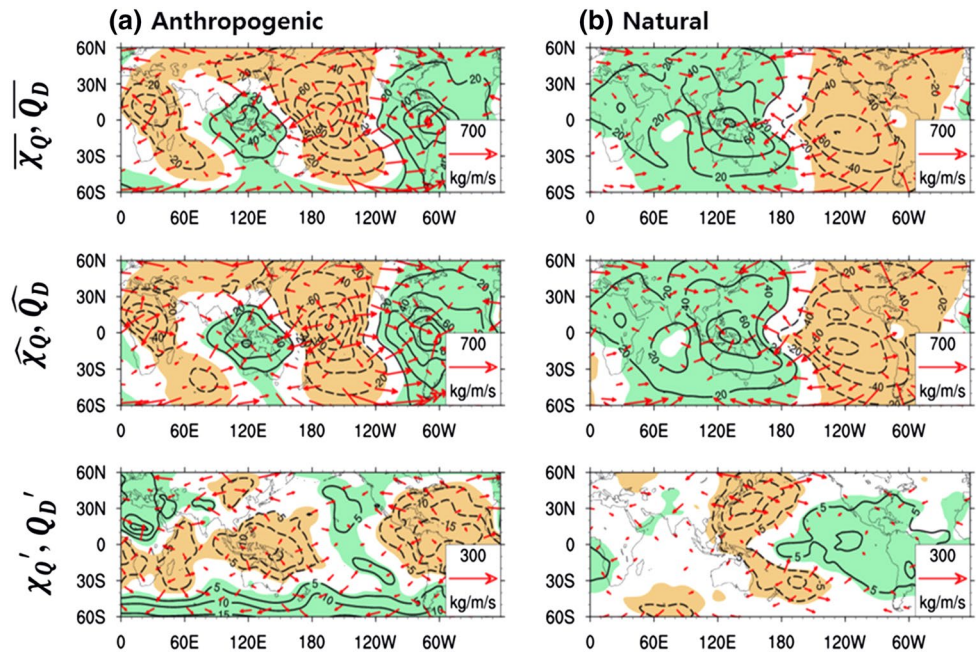
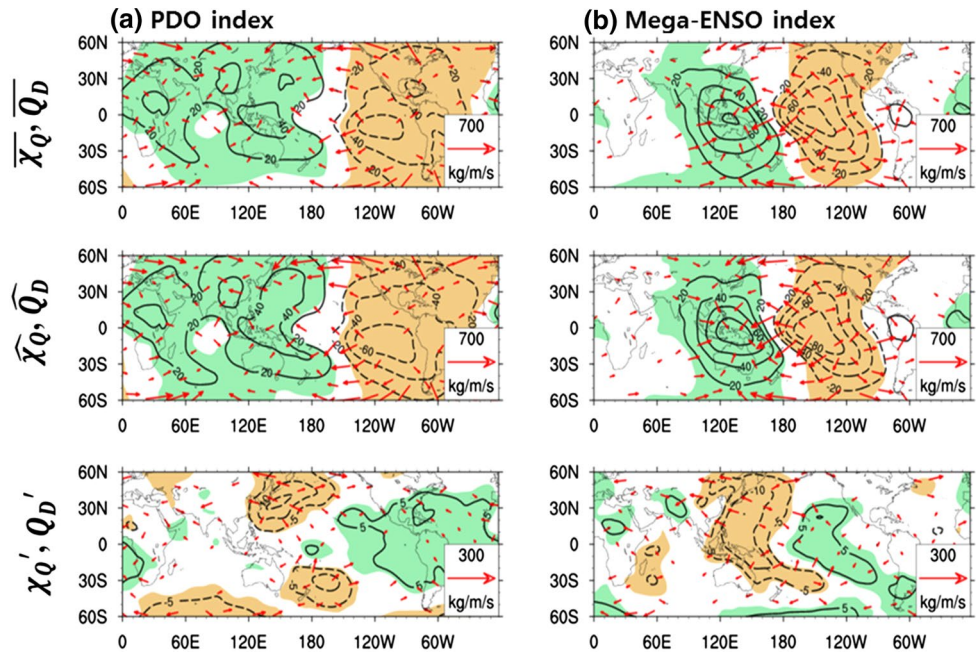


Fig. 5 Same as Fig. 4 except for **a** the negative PDO and **b** mega-ENSO indices



The time-averaged potential function and divergent component of moisture flux divide into stationary and eddy parts:

$$\overline{\chi_Q} = \widehat{\chi_Q} + \chi_Q'$$

$$\overline{Q_D} = \widehat{Q_D} + Q_D'$$

where $\widehat{()}$ is the stationary part and $()'$ is the eddy part. The potential function and divergent component distributions are dominated mostly by the stationary part (Fig. 4).

The eddy part can exert an affect in the middle latitudes, but its effect is also smaller than that of the stationary part.

To compare the decadal variability indices, the negative PDO index and mega-ENSO index were regressed on the potential function and divergent component of moisture flux (Fig. 5). The two indices well show the zonal dipole pattern of the potential function. However, the mega-ENSO index well captures the easterly moisture transport over the tropics, but the negative PDO index does not. This is a

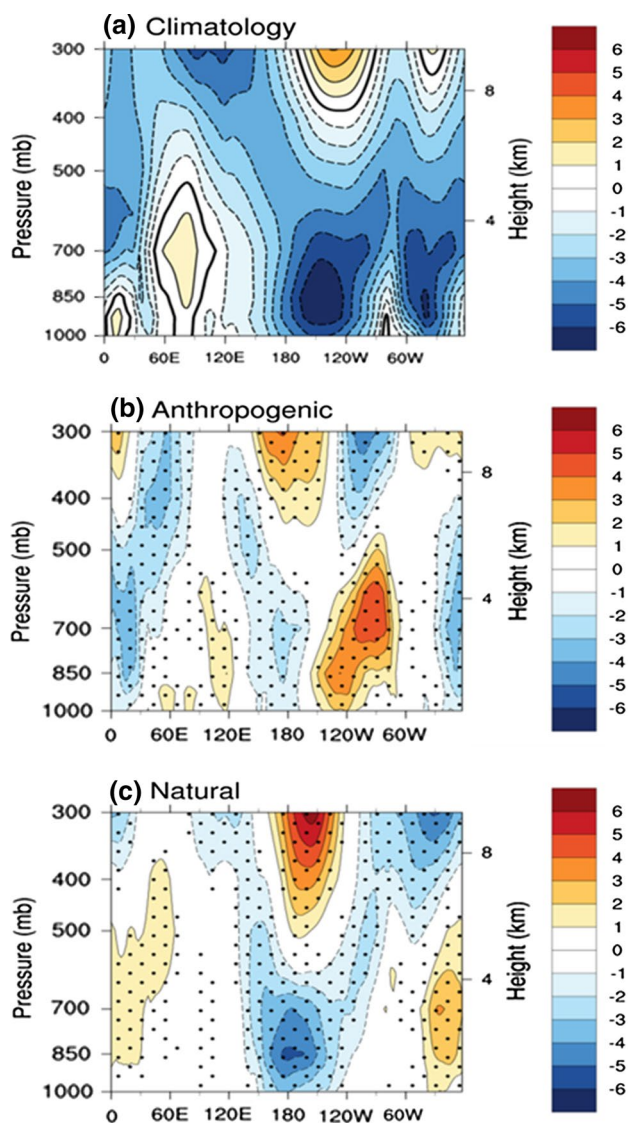


Fig. 6 Longitude–height cross sections of **a** climatology zonal wind (ms^{-1}) and regressed fields of zonal wind (10^2ms^{-1}) onto the PC time series of **b** anthropogenic mode and **c** natural mode at 10°S – 10°N . Stippled areas denote the statistically significant region above the 95 % confidence level by Student’s *t* test

consequence of the PDO index being derived as the leading PC of monthly detrended SST anomalies in the North Pacific Ocean, poleward of 20°N . Thus, the mega-ENSO index is better than the PDO index for denoting characteristics in the tropical Pacific.

To investigate the vertical structure change of zonal wind by anthropogenic and natural forcings, the zonal winds in the tropics [10°S – 10°N] were used. In anthropogenic mode, the anomalous westerly winds at low level strengthen the climatological westerly winds over the Indian Ocean (IO) [60°E – 120°E], while the anomalous westerly winds at low and middle levels weaken the

climatological easterly winds over the EP (Fig. 6a, b). In particular, over the EP, the anthropogenic forcing has a vertically elongated significant effect up to 500 hPa. As a result, the Walker circulation is hindered by anthropogenic forcing. Vecchi and Soden (2006) detected a robust signal of weakening Walker circulation under global warming using climate models. In natural mode, the easterly winds are enhanced by the anomalous easterly winds at low level over the CP (Fig. 6c). This strengthened easterly wind over the CP can contribute to a strengthening of the Walker circulation. However, if the decadal ENSO is in El Niño phase, the effect of natural variability counteracts the Walker circulation. Therefore, during the recent three decades, the increased precipitation over the WP seems a result of the combination of a strengthened westerly wind over the IO by anthropogenic forcing and a strengthened Walker circulation over the Pacific by natural variability, despite the disturbance of anthropogenic forcing. However, many works have shown evidences that following the global warming driven by the greenhouse gas forcing, an easterly wind anomaly will appear in the IO (Chu et al. 2014; Dong and Zhou 2014a; Dong et al. 2014). In future projection using the models, the warmer SST is appeared over the western IO. However, in this study, the SST pattern is similar a basin wide pattern. Thus, the westerly wind anomaly seems to be led by zonal SST gradient. Also, the Kelvin-Rossby waves can lead the westerly wind anomaly (Lau and Peng 1987; Hendon 1988; Rui and Wang 1990), but the cause and effect can’t prove because the annual mean variables are used. The mechanism related to the wind in global warming will investigated in the further study.

5 Summary and discussion

This study aimed to investigate the changes in observed precipitation and moisture transport by anthropogenic forcing and natural variability. To better understand the change in precipitation, the major components of the moisture budget, including moisture flux convergence, were investigated based on several reanalysis data.

The SVDs of precipitation and SST are not sufficient to divide into anthropogenic and natural modes because moisture is directly affected by SST whereas precipitation patterns are controlled by wind circulation. Thus, in this study, the MVEOF synthesized from the three variables of precipitation, SST, and CVIMF was used to consider the dynamic and thermodynamic factors. As a result, the anthropogenic and natural modes were well separated by MVEOF analysis. The anthropogenic mode showed a tri-polar distribution of precipitation over the tropics. The natural variability strengthened the zonal asymmetric precipitation near 150°E . The change in CVIMF well

matched the change in precipitation by the two forcings, particularly over the tropics. Thus, precipitation change can be estimated by moisture transport. The dynamic component of the moisture flux dominates precipitation change induced by anthropogenic forcing and natural variability. The dynamic component affects the long-term trend and interannual variability of global monsoon rainfall (Lin et al. 2014). Thus, the dynamic component is important in variation of precipitation.

To better understand the changes in moisture source and sink regions associated with increased and decreased precipitation, we investigate the potential function and divergent component of moisture flux. Through the moisture budget analysis, it was identified that the anthropogenic mode has zonal wavenumber 2 structure of the potential function and that the natural mode has zonal wavenumber 1 structure divided at the dateline. A common feature of the two modes is a dominant zonal moisture transport by the divergent component over the tropics. Additionally, we identified that the mega-ENSO index indicates decadal variability of SST better than the PDO index through the divergent component of moisture flux. When the decadal ENSO is in La Niña phase, the natural and anthropogenic modes show a positive sign of potential function, which denotes an increase of precipitation over the tropical WP. In the tropics, anthropogenic mode shows significant anomalous westerly winds over the IO and EP, while the anomalous easterly winds over the WP. The natural mode has significant anomalous easterly winds over the CP. In particular, under a global warming scenario, the anomalous westerly winds over the EP denote a vertically elongated effect to the middle as well as the low level of the atmosphere. The anomalous easterly winds of natural mode have more strength than the anomalous westerly winds of anthropogenic mode over the tropical Pacific at low level. Therefore, the recent increase in moisture convergence over the tropical WP can be explained by the strengthened westerly and easterly winds near the WP by anthropogenic forcing and the strengthened easterly winds over the Pacific by natural variability at low level because the moisture is almost entirely transported at low level. However, the cause of winds over the IO is unclear in this study. The Kelvin-Rossby waves can lead to the changes in zonal winds over the tropics. Thus, the part is remained for the further study.

Although we used the ensemble mean to reduce the uncertainty between several datasets, this study may still include uncertainty related to the reliability of the reanalysis data because of uncertain satellite measurements associated with algorithm defects or calibration errors. Nevertheless, the increase in precipitation over the WP is a robust result compared to previous modeling studies under global warming (Chou and Neelin 2004; Held and Soden 2006;

Chou et al. 2009). Also, a definite answer to the question of whether natural variability, as well as global warming, plays a significant role in long-term precipitation change is presented in this study. Therefore, the knowledge presented here is helpful for understanding the driving factors of past and future change in global precipitation patterns and the dynamics of the hydrological cycle. It also has important ramifications for decadal prediction of precipitation pattern change, which is critical for water resource management, agriculture, extreme hydrological disaster prevention, and infrastructure planning.

Acknowledgments This work was supported by GRL grant of the National Research Foundation (NRF) funded by the Korean Government (NRF-2011-0021927). We would like to express our sincere thanks to Prof. Bin Wang for his insightful comments. The comments and suggestions of two anonymous reviewers are greatly appreciated.

References

- Chen TC (1985) Global water vapor flux and maintenance during FGGE. *Mon Weather Rev* 113:1801–1919
- Chen M, Xie P, Janowiak JE, Arkin PA (2002) Global land precipitation: a 50-yr monthly analysis based on gauge observation. *J Hydrometeorol* 3:249–266
- Cherchi A, Alessandri A, Masina S, Navarra A (2011) Effects of increased CO₂ levels on monsoons. *Clim Dyn* 37:83–101
- Chou C, Neelin JD (2004) Mechanisms of global warming impacts on regional tropical precipitation. *J Clim* 17:2688–2701
- Chou C, Neelin JD, Chen CA, Tu JY (2009) Evaluating the “rich-get-richer” mechanism in tropical precipitation change under global warming. *J Clim* 22:1982–2005
- Chu JE, Ha JK, Lee JY, Wang B, Kim BH, Chung CE (2014) Future change of the Indian Ocean basin-wide and dipole modes in the CMIP5. *Clim Dyn* 43:551–553
- Cobb KM, Charles CD, Cheng H, Edwards RL (2003) El Niño/Southern oscillation and tropical Pacific climate during the last millennium. *Nature* 424:271–276
- Dee D et al (2011) The ERA-interim reanalysis: configuration and performance of the data assimilation system. *Q J R Meteorol Soc* 137:553–597
- Dong L, Zhou T (2014a) The Indian Ocean sea surface temperature warming simulated by CMIP5 models during the 20th century: competing forcing roles of GHGs and anthropogenic aerosols. *J Clim* 27:3348–3362
- Dong L, Zhou T (2014b) The formation of the recent cooling in the eastern tropical Pacific Ocean and the associated climate impacts: a competition of global warming, IPO, and AMO. *J Geophys Res* 119:272–287
- Dong L, Zhou T, Wu B (2014) Indian Ocean warming during 1958–2004 simulated by a climate system model and its mechanism. *Clim Dyn* 42:203–217
- Held IM, Soden BJ (2006) Robust responses of the hydrological cycle to global warming. *J Clim* 19:5686–5699
- Hendon (1988) A simple model of the 40–50 day oscillation. *J Atmos Sci* 45:569–584
- Higgins RW et al (2003) Progress in pan American CLIVAR research: the North American monsoon system. *Atmosfera* 16:30–65
- Hoerling M, Eischeid J, Perlwitz J (2010) Regional precipitation trends: distinguishing natural variability from anthropogenic forcing. *J Clim* 23:2131–2145

- Hsu PC, Li T, Wang B (2011) Trends in global monsoon area and precipitation over the past 30 years. *Geophys Res Lett* 38:L08701
- Hsu PC, Li T, Luo JJ, Murakami H, Kitoh A, Zhao M (2012) Increase of global monsoon area and precipitation under global warming: A robust signal? *Geophys Res Lett* 39:L06701
- Kalnay E et al (1996) The NCEP/NCAR 40-year reanalysis project. *Bull Am Meteor Soc* 77:437–471
- Lau and Peng (1987) Origin of low-frequency (intraseasonal) oscillations in the tropical atmosphere. Part 1: basic theory. *J Atmos Sci* 44:950–972
- Lee JY, Wang B (2014) Future change of global monsoon in the CMIP5. *Clim Dyn* 42:101–119
- Lee EJ, Ha KJ, Jhun JG (2014) Interdecadal changes in interannual variability of the global monsoon precipitation and interrelationships among its subcomponents. *Clim Dyn* 42:2585–2601
- Lin R, Zhou T, Qian Y (2014) Evaluation of global monsoon precipitation changes based on five reanalysis datasets. *J Clim* 27:1271–1289
- Liu J, Wang B, Cane MA, Yim SY, Lee JY (2013) Divergent global precipitation changes induced by natural versus anthropogenic forcing. *Nature* 493:656–659
- Marvel K, Bonfils C (2013) Identifying external influences on global precipitation. *PNAS*. doi:10.1073/pnas.1314382110
- McBride JL (1987) The Australian summer monsoon. In: Chang C-P, Krishnamurti TN (eds) *Monsoon meteorology*. Oxford University Press, Oxford, pp 203–231
- Nicholson SE, Kim E (1997) The relationship of the El Niño Southern oscillation to African rainfall. *Int J Climatol* 17:117–135
- Parker DE, Rayner NA, Horton EB, Folland CK (1999) Development of the Hadley Centre sea ice and sea surface temperature data sets (HadISST). WMO workshop on advances in marine climatology-CLIMAR99, Vancouver, BC, Canada, Environment Canada, pp. 194–203
- Polson D, Hegerl GC, Zhang X, Osborn TJ (2013) Causes of robust seasonal land precipitation changes. *J Clim* 26:6679–6697
- Ropelewski CF, Halpert MS (1996) Quantifying Southern oscillation-precipitation relationships. *J Clim* 9:1043–1059
- Rosen RD, Salstein DA, Peixoto JP (1979) Variability in the annual fields of large-scale atmospheric water vapor transport. *Mon Weather Rev* 107:26–37
- Rui H, Wang B (1990) Development characteristics and dynamic structure of tropical intraseasonal convection anomalies. *J Atmos Sci* 47:357–379
- Seager R, Naik N, Vecchi GA (2010) Thermodynamic and dynamic mechanisms for large-scale changes in the hydrological cycle in response to global warming. *J Clim* 23:4651–4668
- Smith TM, Reynolds RW, Peterson TC, Lawrimore J (2008) Improvements to NOAA's historical merged land-ocean surface temperature analysis (1880–2006). *J Clim* 21:2283–2296
- Sohn BJ, Smith EA, Robertson FR, Park SC (2004) Derived over-ocean water vapor transports from satellite-retrieved E-P datasets. *J Clim* 17:1352–1365
- Tao S, Chen L (1987) A review of recent research on the East Asian summer monsoon in China. In: Chang CP, Krishnamurti TN (eds) *Monsoon meteorology*. Oxford University Press, Oxford, pp 60–92
- Trenberth KE, Guillemot CJ (1995) Evaluation of the global atmospheric moisture budget as seen from analyses. *J Clim* 8:2255–2272
- Uppala SM et al (2005) The ERA-40 reanalysis. *Q J R Meteorol Soc* 131:2961–3012
- Vecchi GA, Soden B (2006) Global warming and the weakening of the tropical circulation. *J Clim* 20:4316–4340
- Wang B, Ding QH (2006) Changes in global monsoon precipitation over the past 56 years. *Geophys Res Lett* 33:L06711. doi:10.1029/2005GL025347
- Wang B, Liu J, Kim HJ, Webster PJ, Yim SY (2012) Recent change of the global monsoon precipitation (1979–2008). *Clim Dyn* 39:1123–1135
- Wang B, Liu J, Kim HJ, Webster PJ, Yim SY, Xiang B (2013) Northern Hemisphere summer monsoon intensified by mega-El Niño southern oscillation and Atlantic multidecadal oscillation. *PNAS*. doi:10.1073/pnas.1219405110
- Webster PJ, Magana VO, Palmer TN, Shukla J, Tomas RA, Yanai M, Yasunari T (1998) Monsoon: processes, predictability, and the prospects for prediction. *J Geophys Res* 103:14451–14510
- Yun KS, Seo KH, Ha KJ (2010) Interdecadal change in the relationship between ENSO and the intraseasonal oscillation in East Asia. *J Clim* 23:3599–3612
- Zhou JY, Lau KM (1998) Does a monsoon climate exist over South America? *J Clim* 11:1020–1040